THE JOURNAL OF PHYSICAL CHEMISTRY A

Article

pubs.acs.org/JPCA

Temperature-Dependent Kinetics Study of the Reactions of OH with C_2H_5I, *n*-C_3H_7I, and iso-C_3H_7I

Shaoliang Zhang,[†,‡] Rafal S. Strekowski,*[,†,§] Anne Monod,[†,§] Loïc Bosland,[‡] and Cornelius Zetzsch[∥]

[†]Laboratoire Chimie Environment, Aix-Marseille Université, 13331 Marseille cedex 03, France,

[‡]Institut de Radioprotection et de Sûreté Nucléaire, DPAM/SEMIC/LETR, Centre de Cadarache, 13115 Saint Paul les Durance cedex, France

[§]CNRS, FRE 3416, 13331 Marseille cedex 03, France

[∥]Atmospheric Chemistry Research Laboratory, BAYCEER, University of Bayreuth, Dr. Hans-Frisch-Strasse 1-3, D-95448 Bayreuth, Germany

ABSTRACT: Flash photolysis (FP) coupled with resonance fluorescence (RF) was used to measure the absolute rate coefficients for the reactions of OH($X^2\Pi$) radicals with C_2H_5I (k_1), *n*-C_3H_7I (k_2), and iso-C_3H_7I (k_3) at temperatures between 297 and 372 K in 188 Torr of He; this represents the first temperature-dependent kinetics studies for the title reactions. The experiments involved time-resolved RF detection of the OH ($A^2\Sigma^+ \rightarrow X^2\Pi$ transition at λ = 308 nm) radicals following FP of H_2O/C_2H_5I/He, H_2O/*n*-C_3H_7I/He, and H_2O/iso-C_3H_7I/He mixtures. The OH($X^2\Pi$) radicals were produced by FP of H_2O in vacuum-UV at wavelengths λ > 120 nm. Decays of OH radicals in the presence of C_2H_5I, *n*-C_3H_7I, and iso-C_3H_7I were observed to be exponential, and the decay rates were found to be linearly dependent on the C_2H_5I, *n*-C_3H_7I, and iso-C_3H_7I concentrations. The results are described by the following Arrhenius expressions (units of cm^3 $molecule^{-1}$ s^{-1}): $k_1(297–372\ K) = (5.55 \pm 3.20) \times 10^{-12} \exp[-(830 \pm 90)\ K/T]$, $k_2(300–370\ K) = (1.65 \pm 0.90) \times 10^{-11} \exp[-(780 \pm 90)\ K/T]$ and $k_3(299–369\ K) = (7.58 \pm 3.70) \times 10^{-12} \exp[-(530 \pm 80)\ K/T]$. Reported errors in E/R and in the pre-exponential factors are 2σ random errors, returned by the weighted (by $1/\sigma^2$) least-squares fits to the kinetic data. The implications of the reported kinetic results for understanding both atmospheric and nuclear safety interests of C_2H_5I, *n*-C_3H_7I, and iso-C_3H_7I are discussed.

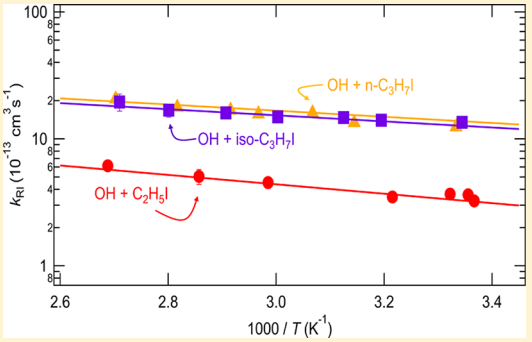

INTRODUCTION

The potential importance of iodine in tropospheric chemistry was suggested by Chameides and Davis (1980),[1] and there is now increasing evidence that chain processes involving reactive halogen radicals, namely, I and IO radicals, play a non-negligible role in tropospheric ozone loss.[2,3] For example, an atmospheric IO mixing ratio of 6 ppt[4] was shown to increase the boundary-layer ozone loss rate by as much as 70% over the ocean and 10% over land.[5] Further, it has been suggested that atmospheric IO radicals modulate the tropospheric ratios of NO_2 to NO and HO_2 to OH.[4,6] A shift in the HO_2/OH ratio occurred that resulted in a 9% increase in tropospheric OH radical concentration when I-atom mixing ratios of 7 ppt were observed in the upper troposphere.[6]

In the atmosphere, IO radicals are formed in the reaction of I atoms with O_3. In turn, I atoms are formed following photolysis and oxidative attack of iodoalkanes by atmospheric radicals, namely, OH, O, and Cl during the day and NO_3 at night. Iodoalkanes are mostly formed in the marine environment by various types of macroalgae and microalgae (phytoplankton).[7] Further, it has been suggested that, independent of biogenic generation, iodoalkanes are formed chemically in the presence of atmospheric ozone, dissolved iodide, and organic matter.[8] Methyl iodide (CH_3I), diiodomethane (CH_2I_2), iodoethane (C_2H_5I), 1-iodopropane (*n*-C_3H_7I), and 2-iodopropane (iso-C_3H_7I) are key iodoalkanes of biogenic and photochemical origins that appear to be of central importance in understanding iodine chemistry in the marine boundary layer (MBL). Whereas CH_3I and more recently CH_2I_2 have received most of the attention in efforts to better understand MBL iodine chemistry, the source strengths of other iodine-containing compounds, namely, C_2H_5I, *n*-C_3H_7I, and iso-C_3H_7I, could exceed that of CH_3I.[9] Field observations in the Arctic suggest that iso-C_3H_7I mixing ratios could be as high as 2 pptv,[10] and both *n*-C_3H_7I, and iso-C_3H_7I were detected in Arctic seawater samples.[3,10]

Atmospheric loss processes for C_2H_5I, *n*-C_3H_7I, and iso-C_3H_7I include photolysis and gas-phase reactions with OH radicals,[11,12] O(^{3}P) radicals,[13] and Cl atoms.[5,14] Because the absorption spectra of iodoalkanes extend well into the actinic region, the atmospheric fate of iodoalkanes is mostly governed by photolysis releasing iodine atoms into the atmosphere.[15−17]

Received: January 17, 2012
Revised: August 12, 2012
Published: August 13, 2012

dx.doi.org/10.1021/jp300575f | *J. Phys. Chem. A* 2012, 116, 9497−9506

However, monosubstituted iodoalkanes, namely, C_2H_5I, *n*-C_3H_7I, and iso-C_3H_7I, have much longer photolytic lifetimes than multiply substituted iodoalkanes. As a result, the reactions of OH with C_2H_5I, *n*-C_3H_7I, and iso-C_3H_7I could compete with photolysis.

In addition to atmospheric interest, the reactivity of organic iodides has recently gained increased interest in the field of nuclear industry safety in efforts to better understand chemical processes responsible for the formation of molecular iodine and iodine oxides resulting from a severe nuclear power plant accident of the type in Fukushima, Japan. Among all possible "released" fission products, volatile iodine has the highest radiological health impact; specifically, the isotope ^{131}I is known to bind to the thyroid gland. Organic iodides are a particularly volatile form of the fission product iodine (I_2) that are difficult to retain by postaccident filtration systems.[18] The quantity of volatile iodine-containing compounds, namely, I_2, organic iodides, and iodine oxides, that would be released to the environment is, therefore, a major security and public health issue. To better understand the nature and quantities of radioactive products released to the environment under conditions of a severe nuclear power plant accident, several experimental programs, including a large-scale international Phebus Fission Product (FP) program (PHEBUS FP) and other intermediate- and smaller-scale projects, were launched in the late 1980s to study nuclear power plant reactor core degradation, the transport of fission products, and the release of fission products into the reactor containment volume. The international PHEBUS FP program reproduces (on a reduced scale 1/5000 versus 900 MW pressurized water reactor [PWR]) a core meltdown accident in a PWR. The continuous objective of the PHEBUS FP program is to reduce the uncertainty in the speciation and quantity of fission products that could be released into the environment if a major nuclear power plant accident were to occur. One of the results of this program is that short-chain organic iodides are formed such as CH_3I, CH_2I_2, C_2H_5I, *n*-C_3H_7I, and iso-C_3H_7I, under irradiation from various building surfaces of the reactor containment area. More recently, the Nuclear Energy Agency (NEA) Committee for the Safety of Nuclear Installations (CSNI) launched the Behavior of Iodine Project (BIP), which identified other longer-chain alkyl iodides that would be released into the environment if a major nuclear power plant accident were to occur.[18] Under conditions in the head space of the reactor in the event of a major nuclear power plant accident, that is, 80 °C < T < 150 °C and ≥60% relative humidity, the fate of the released organic iodides will be governed by destruction by β- and γ-radiation and complex mechanisms involving air and steam radiolysis products, namely, hydroxyl radicals, OH($\Sigma^2\Pi$), and oxygen radicals [O(^{3}P)], among others.[19−21] However, given the large mixing ratios of ozone and the very high relative humidity found in the containment volume of the nuclear power plant building following a severe nuclear power plant accident, the destruction of organic iodides by OH($\Sigma^2\Pi$) and O(^{3}P) radicals could compete with destruction by β- and γ-radiation. The products of the destruction of organic iodides are believed to be iodine oxides that are known to form aerosols. However, to date, the mechanisms and kinetics of the destruction and formation of many organic iodides remain uncertain and unknown. The ability of the nuclear safety field measurement community to accurately determine the concentrations of reactive free radicals has evolved to the point where detailed comparisons of experimental data with calculation codes used in the study of the evolution of serious accidents and their consequences is limited by the accuracy and availability of rate coefficients for key reactions. For this reason, new kinetic studies of important chemical processes that focus on high accuracy are needed. Because one of the major oxidant products from air radiolysis under nuclear power plant accident conditions is OH radicals, there is a need to carry out kinetic and mechanistic studies of the reaction of OH radicals with selected organic iodides (RIs) to better evaluate their destruction that is supposed to lead to the formation of iodine oxide aerosols through IO formation.

To date, only two laboratory studies report on the room-temperature rate constants for the reactions of OH radicals with C_2H_5I, *n*-C_3H_7I, and iso-C_3H_7I with somewhat different results.[11,22] No temperature-dependent data have been reported in the literature for the reactions OH + C_2H_5I, OH + *n*-C_3H_7I, and OH + iso-C_3H_7I. As a result, the aim of this work was to determine the rate coefficients for the reactions of OH radicals with C_2H_5I, $k_1(T)$; *n*-C_3H_7I, $k_2(T)$; and iso-C_3H_7I, $k_3(T)$, as functions of temperature

$$OH + C_2H_5I \rightarrow \text{products} \quad (1)$$

$$OH + n\text{-}C_3H_7I \rightarrow \text{products} \quad (2)$$

$$OH + \text{iso-}C_3H_7I \rightarrow \text{products} \quad (3)$$

The total rate coefficients for OH removal by C_2H_5I, *n*-C_3H_7I, and iso-C_3H_7I are reported at temperatures between 297 and 372 K in 188 Torr of He. Details of the experimental approach are provided in the next section.

EXPERIMENTAL APPROACH

The experimental approach is similar to that employed in other studies of OH radical reactions of atmospheric interest.[23−25] The experiments involved time-resolved detection of OH radicals by resonance fluorescence ($A^2\Sigma^+ \rightarrow X^2\Pi$) at λ = 308 nm following vacuum-UV (VUV) flash photolysis of H_2O/C_2H_5I/He, H_2O/*n*-C_3H_7I/He, H_2O/iso-C_3H_7I/He, and H_2O/He mixtures.[26] A schematic diagram of the flash photolysis resonance fluorescence (FPRF) apparatus is shown in Figure 1, and some experimental details that are particularly relevant to this work are discussed next.

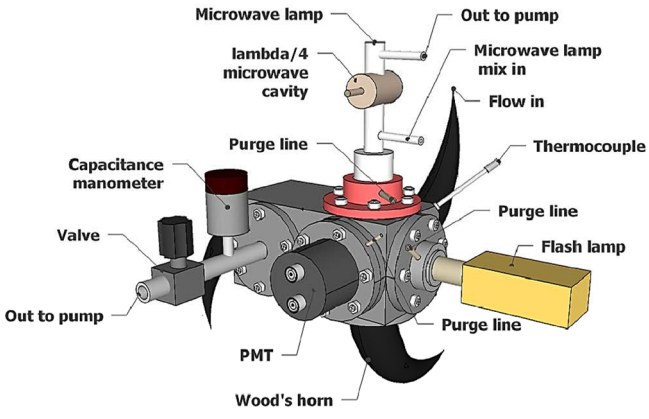

Figure 1. Schematic representation of the flash photolysis resonance fluorescence (FPRF) apparatus used to study the reaction of OH radicals with C_2H_5I, *n*-C_3H_7I, and iso-C_3H_7I. PMT: Photomultiplier tube.

A black anodized aluminum reaction cell was used in all experiments carried out under precise temperature, pressure, and flow conditions. The reaction cell was maintained at a constant temperature (±1 K) using a heating ribbon (FGR Series, Newport Omega) connected to a temperature controller (CN400 Series, Newport Omega), and the temperature within the reactor was monitored using a type-J thermocouple. The reaction cell and the gas saturation system are similar to those described in detail by Witte et al.[27] and Wahner and Zetzsch.[28] The geometry of the reaction vessel was such that it allowed for the VUV beam and the resonance lamp beam to enter perpendicular to one another and to the photomultiplier (i.e., the RF detector), to be orthogonal to the two overlapping beams. The direction of gas flow was perpendicular to the direction of propagation of both the photolysis VUV beam and the probe radiation beam.

In all experiments, a Perkin-Elmer FX 1165 short arc xenon flashlamp with a < 200 ns flash jitter served as the photolytic light source. The reactant OH($X^2\Pi$) was generated through FP of H_2O. Flash energies ranged from ∼506 to ∼674 mJ. Flash energy was calculated based on the discharge capacitance and input voltage. The VUV beam entered the reaction cell through a MgF_2 window. A resonance lamp mounted at a right angle to the VUV photolysis excited the photolytically produced OH radicals in the reaction cell by resonance fluorescence. The resonance lamp consisted of a 150 mm × 12 mm outer diameter fused silica tube fitted with a silver-plated microwave cavity[29] (Opthos Instruments, Inc.) powered by a microwave generator (Muegge, Reichelsheim, MW-GPRYJ1511-300-01, 2.45 GHz, 300 W) and operated at ∼70 W. A gas mixture of ∼0.1% H_2O/He at a total pressure of a few Torr was allowed to flow through the resonance lamp. The electrodeless microwave discharge dissociates H_2O and creates OH radicals. These radicals are then electronically excited to the $A^2\Sigma^+$ state through collisions with either electronically excited helium or free electrons. Because fluorescence is resonant, the $A^2\Sigma^+ \rightarrow X^2\Pi$ radiation leaving the lamp electronically excites OH($X^2\Pi$) radicals present in the reaction vessel. The resulting resonant fluorescence ($A^2\Sigma^+ \rightarrow X^2\Pi$) at 308 nm is coupled out of the lamp through a quartz lens (Heraeus, Suprasil, f_{VIS} = 50 mm) into the reaction cell. The resonance fluorescence light is collected by another antireflection-coated quartz lens (Heraeus, Suprasil, f_{VIS} = 50 mm); passes through two 308-nm interference filters (fwhm, 9 nm each), which block any impurity emissions from the resonance lamp radiation and stray light on the axis normal to both the photolysis VUV beam and the resonance lamp beam; and is imaged by another quartz lens (Heraeus, Suprasil, f_{VIS} = 50 mm) onto the photocathode of a photomultiplier tube (Thorn-EMI, 9789QB). Dry nitrogen gas was used to prevent room air from entering the volume between the flash lamp and the reaction cell. The signal was processed using photon-counting techniques in conjunction with multichannel scaling (EG&G Ortec, model ACE MCS) and accumulated in a PC.

All experiments were carried out under "slow flow" conditions and a low VUV repetition rate of 0.3 Hz in order to replenish the gas mixture within the detection volume between VUV flashes. The reactor temperature was varied between 297 and 372 K in 188 Torr He buffer.

The gases used in this study had the following stated minimum purities: He (Linde Gas), 99.9999%; N_2 (Linde Gas), 99.9995%. The liquids used in this work had the following stated minimum purities: C_2H_5I (Sigma Aldrich), 99%; n-C_3H_7I (Sigma Aldrich), 99%; and iso-C_3H_7I (Sigma Aldrich), 99%. To limit iodoalkane decomposition, the liquid samples were stored under dark conditions at 6 °C. Deionized water (resistivity > 18 MΩ) was prepared by passing tap water through a reverse-osmosis demineralization filter (ATS Groupe Osmose), followed by a commercial deionizer (Millipore, Milli-Q).

Concentrations of H_2O, C_2H_5I, n-C_3H_7I, and iso-C_3H_7I in the reaction mixture were calculated from the given vapor pressures, mass flow rates, and total pressure. The Antoine equation for H_2O used in this study is $\log_{10}[P(\text{bar})] = 5.40221 - \{1838.675/[T(\text{K}) + (-31.7)]\}$.[30] The Antoine equation for C_2H_5I used in this study is $\log_{10}[P(\text{bar})] = 7.26806 - \{1396.07/[T(\text{K}) + (-245.911)]\}$.[31] The saturator that contained the C_2H_5I sample was maintained at $T(°\text{C}) = -1.0 \pm 0.5$. The Antoine equation for n-C_3H_7I used in this study is $\log_{10}[P(\text{bar})] = 7.22121 - \{1507.41/[T(\text{K}) + (-244.701)]\}$.[31] The saturator that contained the n-C_3H_7I sample was kept at $T(°\text{C}) = 0.0 \pm 0.5$. The Antoine equation for iso-C_3H_7I used in this study is $\log_{10}[P(\text{bar})] = 7.0167 - \{1340.448/[T(\text{K}) + (-234.365)]\}$.[31] The saturator that contained the iso-C_3H_7I sample was maintained at $T(°\text{C}) = -6.0 \pm 0.5$.

The initial OH radical concentration was not directly measured but was determined experimentally at room temperature using the water-vapor UV-photolysis calibration technique and oxygen actinometry as described in detail by Dusanter et al.[32] and Faloona et al.[33] Briefly, this technique uses direct photolysis of water vapor at atmospheric pressure. It was assumed that the photolysis of water leads to the production of equal amounts of OH radicals and H atoms

$$H_2O + h\nu \rightarrow OH + H \quad (4)$$

The initial hydroxyl radical concentration, $[OH]_0$, was calculated from the relationship[32,33]

$$[OH]_0 = \Phi_{OH}\sigma_{H_2O}[H_2O]Ft \quad (I)$$

where Φ_{OH} is the quantum yield for the OH radical production from VUV photolysis of H_2O, σ_{H_2O} is the absorption cross section for H_2O, F is the flash lamp fluence, and t is the photolysis time. It was assumed that $\Phi_{OH} = 1$.[34] The absorption cross section for H_2O, σ_{H_2O}, varies between 0.5×10^{-18} and 8×10^{-18} cm^2 in the wavelength range from 120 to 180 nm.[35] As in the work of Rinke and Zetzsch,[25] we used $\sigma_{H_2O} = 5 \times 10^{-18}$ cm^2.

In eq I, the product Ft is derived from oxygen actinometry by measuring the concentration of ozone using a commercial ozone analyzer (Environment S.A., O_3 41M) following VUV photolysis of a 20% O_2/N_2 reaction mixture[36,37]

$$[O_3] = \Phi_{O_2}\sigma_{O_2}[O_2]Ft \quad (II)$$

where $\Phi_{O_2} = 2$ is the photolysis quantum yield and σ_{O_2} is the absorption cross section for O_2.

Equation II can be rewritten to give the product Ft

$$Ft = \frac{[O_3]}{2[O_2]\sigma_{O_2}} \quad (III)$$

The absorption cross section for O_2, σ_{O_2}, varies between 2×10^{-17} and 8×10^{-17} cm^2 in the wavelength range from 120 to 180 nm.[35] In this work, σ_{O_2} was taken to be 5×10^{-17} cm^2.[35] Substituting the product Ft from eq III into eq I gives $[OH]_0$.

dx.doi.org/10.1021/jp300575f | J. Phys. Chem. A 2012, 116, 9497−9506

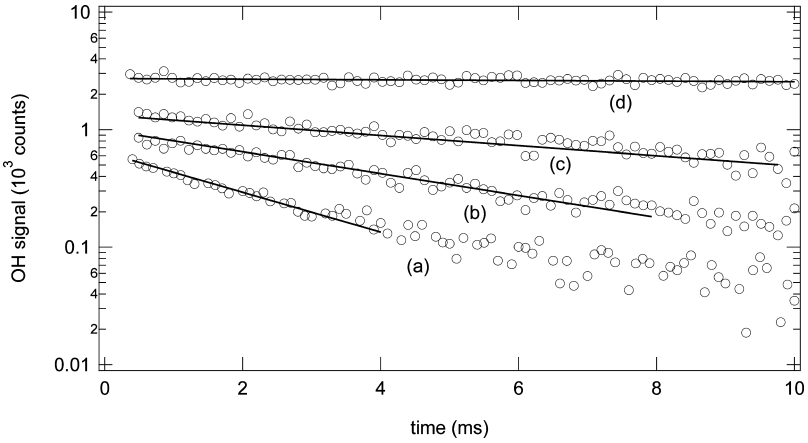

Figure 2. Typical OH radical decay profiles as a function of C_2H_5I concentration ($[C_2H_5I]$). Experimental conditions: T = 297 K; $[H_2O]$ = 1.53 × 10^{15} cm^{-3}; $[C_2H_5I]$ = (a) 0, (b) 2.01 × 10^{14}, (c) 4.81 × 10^{14}, and (d) 10.0 × 10^{14} cm^{-3}. Sixty flashes averaged for each trace a–d. The quantity plotted on the y axis is total accumulated signal counts, which is proportional to the average number of lamp flashes and the multichannel scalar dwell time (122 μs per channel in all traces shown). Solid lines were obtained from least-squares analyses that gave the following best-fit parameters k' = (a) 14, (b) 91, (c) 186, and (d) 359 s^{-1}. The plots have been displaced vertically for clarity.

At $[O_3] \approx 120$ ppb, we estimate $[OH]_0 \approx 2 \times 10^{10}$ molecules cm^{-3} under the experimental conditions employed.

RESULTS AND DISCUSSION

All experiments were carried out under pseudo-first-order conditions with C_2H_5I, n-C_3H_7I, iso-C_3H_7I, H_2O, and He in excess over OH radicals such that $10^3 \times [OH]_0 < [RI]$, where RI = C_2H_5I, n-C_3H_7I, and iso-C_3H_7I. Data were obtained at temperatures between 297 and 372 K in 188 Torr of He. The OH radical temporal evolution was monitored following VUV flash photolysis of H_2O/RI/He reaction mixtures. The processes that control the temporal evolution of the OH radicals are the following

$$H_2O + h\nu \rightarrow OH + H \quad (4)$$

$$OH + RI \rightarrow \text{products} \quad (1\text{–}3)$$

$$OH \rightarrow \text{loss} \quad (5)$$

Because the concentration of each RI was much larger than the initial OH concentration ($[OH]_0$), it was assumed that the observed OH radical temporal profiles followed the pseudo-first-order rate law

$$\ln \frac{[OH]_0}{[OH]} = k't \quad \text{(IV)}$$

In eq IV, $k' = k_{RI}[RI] + k_0$ and is the experimentally measured decay rate in units of s^{-1}, and the decay rate k_0 is the OH radical disappearance rate in the absence of RI. The value of k_0 is basically the sum of the first-order rate coefficients for the reaction of OH radicals with impurities in the He bath gas and with background impurities that find their way into the reaction mixture through small leaks and/or through diffusion through a small amount of Teflon tubing in the apparatus plumbing and the diffusion of OH radicals out of the detection zone. $OH(X^2\Pi)$ is unreactive toward He and does not react readily with H_2O.[38] Some typical $OH(X^2\Pi)$ temporal profiles observed following flash photolysis of H_2O/C_2H_5I/He mixtures are shown in Figure 2.

The first-order OH radical decays observed following FP of H_2O/n-C_3H_7I/He and H_2O/iso-C_3H_7I/He mixtures were similar to those shown for C_2H_5I in Figure 2. The OH radical signal is observed to be proportional to the OH concentration. In all experiments, the observed OH radical signal in the presence and absence of C_2H_5I, n-C_3H_7I, and iso-C_3H_7I was exponential and displayed a linear dependence on the concentrations of C_2H_5I, n-C_3H_7I, and iso-C_3H_7I. The bimolecular rate coefficients for the removal of OH radicals by C_2H_5I, $k_1(T)$; n-C_3H_7I, $k_2(T)$; and iso-C_3H_7I, $k_3(T)$, were obtained from the variation of k' with the concentrations of C_2H_5I, n-C_3H_7I, and iso-C_3H_7I, respectively, at constant H_2O and He concentrations. Typical second-order plots for the reactions OH + C_2H_5I, OH + n-C_3H_7I, and OH + iso-C_3H_7I are shown in Figures 3–5, respectively.

The Arrhenius expression $k_{RI} = A \exp(-E_a/RT)$ was used to deduce the temperature dependence of reactions 1–3, where k_{RI} is the bimolecular rate coefficient, A is the pre-exponential factor, E_a is the activation energy, and R is the gas constant. A linear relationship was obtained by taking the natural logarithm of the Arrhenius expression and plotting ln k versus $1/T$. The

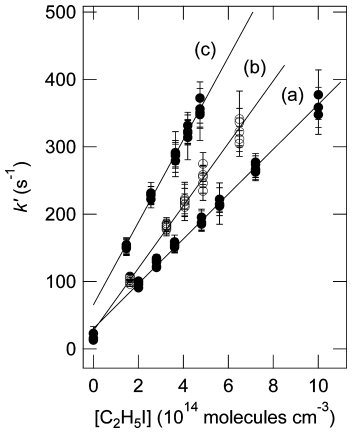

Figure 3. Plots of k' versus C_2H_5I concentration ($[C_2H_5I]$) for data obtained at three different temperatures. Fits were obtained from linear least-squares analyses and give the following bimolecular rate coefficients: (a) (3.24 ± 0.08) × 10^{-13} molecules cm^3 s^{-1} at 297 K, (b) (4.52 ± 0.11) × 10^{-13} molecules cm^3 s^{-1} at 335 K, and (c) (6.13 ± 0.23) × 10^{-13} molecules cm^3 s^{-1} at 372 K. The error bars are 2σ statistical errors in k'.

dx.doi.org/10.1021/jp300575f | J. Phys. Chem. A 2012, 116, 9497–9506

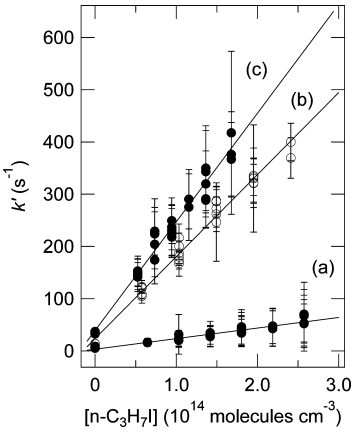

Figure 4. Plots of k' versus n-C_3H_7I concentration ($[n\text{-}C_3H_7I]$) for data obtained at three different temperatures. Fits were obtained from linear least-squares analyses and give the following bimolecular rate coefficients: (a) $(12.4 \pm 0.06) \times 10^{-13}$ molecules cm^3 s^{-1} at 300 K, (b) $(15.7 \pm 1.0) \times 10^{-13}$ molecules cm^3 s^{-1} at 337 K, and (c) $(20.6 \pm 1.6) \times 10^{-13}$ molecules cm^3 s^{-1} at 370 K. The error bars are 2σ statistical errors in k'.

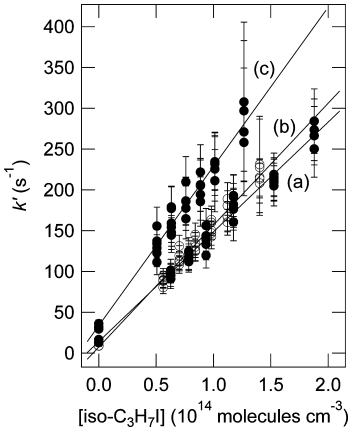

Figure 5. Plots of k' versus iso-C_3H_7I concentration ($[\text{iso-}C_3H_7I]$) for data obtained at three different temperatures. Fits were obtained from linear least-squares analyses and give the following bimolecular rate coefficients: (a) $(13.5 \pm 0.7) \times 10^{-13}$ molecules cm^3 s^{-1} at 299 K, (b) $(14.9 \pm 0.8) \times 10^{-13}$ molecules cm^3 s^{-1} at 333 K, and (c) $(19.5 \pm 3.0) \times 10^{-13}$ molecules cm^3 s^{-1} at 369 K. The error bars are 2σ statistical errors in k'.

values of A and E_a were obtained from the intercept and slope, respectively. The results of all studies of reactions 1−3 are summarized in Table 1, and an Arrhenius plot for the title reactions is shown in Figure 6. The following Arrhenius expressions were derived from the data (units of cm^3 molecule^{-1} s^{-1})

$$k_1(T) = (5.55 \pm 3.20) \times 10^{-12} \exp[-(830 \pm 90)\ \mathrm{K}/T] \quad \text{(V)}$$

$$k_2(T) = (1.65 \pm 0.90) \times 10^{-11} \exp[-(780 \pm 90)\ \mathrm{K}/T] \quad \text{(VI)}$$

$$k_3(T) = (7.58 \pm 3.70) \times 10^{-12} \exp[-(530 \pm 80)\ \mathrm{K}/T] \quad \text{(VII)}$$

The errors in the Arrhenius expressions in eqs V, VI, and VII are 2σ random errors, as obtained by weighted $(1/\sigma^2)$ least-squares fitting to the data listed in Table 1. Assumed

Table 1. Summary of the Kinetic Data for Reactions of OH with C_2H_5I, n-C_3H_7I, and iso-C_3H_7I in 188 Torr of He

T (K)	p (Torr)	[RI] (10^{14} molecules cm^{-3})	k_0[a] (s^{-1})	k'[a] (s^{-1})	k_{RI}[a−c] (10^{-13} cm^3 molecule^{-1}s^{-1})
			C_2H_5I		
297	188	2.01−10.0	14	90−377	3.24 ± 0.08
298	49	0.44−2.35	14	124−202	3.62 ± 0.34[d,e]
301	101	0.65−3.65	10	61−184	3.67 ± 0.26[d,f]
311	188	1.75−6.99	17	91−285	3.48 ± 0.13
335	188	1.63−6.49	16	96−341	4.52 ± 0.11
350	188	1.55−7.74	20	106−414	5.05 ± 0.16
372	188	1.46−4.19	23	150−372	6.13 ± 0.23
			n-C_3H_7I		
300	188	0.64−2.57	15	80−326	12.4 ± 0.6
318	188	0.61−3.63	11	92−499	13.4 ± 0.4
326	57	0.40−1.60	15	117−336	16.0 ± 0.9[d,f]
337	188	0.58−2.41	14	120−400	15.7 ± 1.0
343	91	0.45−1.83	22	103−366	16.8 ± 0.8[d]
355	188	0.55−2.29	22	112−443	17.7 ± 0.6
370	188	0.53−1.68	35	142−418	20.6 ± 1.6
			iso-C_3H_7I		
299	188	0.63−1.88	15	90−284	13.5 ± 0.7
313	251	0.55−1.37	10	81−203	14.0 ± 0.5[d]
320	188	0.58−1.82	11	91−204	14.7 ± 1.0
333	188	0.56−1.82	9	88−231	14.9 ± 0.8
344	140	0.54−1.36	19	102−246	16.0 ± 0.7[d]
357	188	0.52−1.31	21	97−268	16.8 ± 2.0
369	189	0.51−1.26	32	111−307	19.5 ± 3.0

[a] k' (s^{-1}) = k_{RI}[RI] + k_0 and is the experimentally measured decay rate. k_0 (s^{-1}) is the OH radical disappearance rate in the absence of RI. [b] Uncertainty is $\pm 2\sigma$ random errors as returned by least-squares fitting to data such as shown in Figure 2, using 2σ random error in both k' and [RI] as the weighting parameter $(1/\sigma^2)$. [c] Flash energy = 506 mJ; $[H_2O] = 1.50 \times 10^{15}$ molecules cm^{-3}. [d] Flash energy = 674 mJ. [e] $[H_2O] = 1.15 \times 10^{15}$ molecules cm^{-3}. [f] $[H_2O] = 8.20 \times 10^{14}$ molecules cm^{-3}.

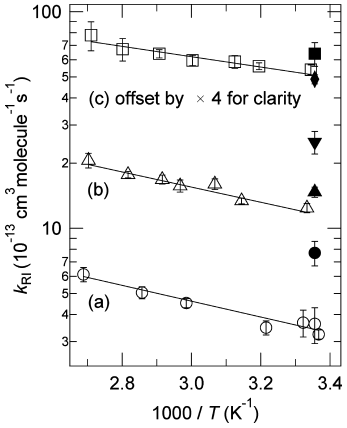

Figure 6. Arrhenius plots for the reactions (a) OH + C_2H_5I, (b) OH + n-C_3H_7I, and (c) OH + iso-C_3H_7I. The solid lines are Arrhenius expressions fitted to the rate constants k_{RI} obtained in this work. The uncertainties are $\pm 2\sigma$, as returned by weighted $(1/\sigma^2)$ least-squares fitting to the data listed in Table 1. Data points ○, ▼, and ■ were taken from Cotter et al. (2003)[22] and correspond to room-temperature reactions OH + C_2H_5I, OH + n-C_3H_7I, and OH + iso-C_3H_7I, respectively. Data points ◆ and ▲ were taken from Carl and Crowley (2001)[11] and correspond to room-temperature reactions OH + n-C_3H_7I and OH + iso-C_3H_7I, respectively.

dx.doi.org/10.1021/jp300575f | J. Phys. Chem. A 2012, 116, 9497−9506

contributions to the overall uncertainty are the random errors; uncertainty in the RI vapor pressure; and small systematic errors in temperature (±1 K), pressure (±1 Torr), and mass flow rates (±1%). At the temperature extremes of the study, the overall uncertainty increases because (a) precision is not as good as at room temperature and (b) uncertainty of ±2 °C in the temperature leads to additional uncertainly in the reactant concentration. We estimate the overall uncertainly in the rate coefficients measured at the higher temperatures of the study to be ±15% at the 95% confidence level.

The room-temperature rate coefficients for the reactions OH + C_2H_5I, OH + n-C_3H_7I, and OH + iso-C_3H_7I obtained in this work and in other studies are compared in Table 2. We found

Table 2. Comparison of Reported Room-Temperature Rate Coefficients for the Reactions OH + C_2H_5I, OH + n-C_3H_7I, and OH + iso-C_3H_7I.a

ref	method[a]	p (Torr)	k_{RI} (10^{-13} cm^3 molecule^{-1} s^{-1})
		C_2H_5I	
Cotter et al.[22]	FFD-RF	1.5 and 5.0 (He)[b]	7.7 ± 1.0
this work	FP-RF	188 (He)[b]	3.4 ± 0.4
		n-C_3H_7I	
Carl and Crowley[11]	LFP-RF	20 (Ar)[b]	14.7 ± 0.8
Cotter et al.[22]	FFD-RF	1.5 and 5.0 (He)[b]	25 ± 3
this work	FP-RF	188 (He)[b]	12.0 ± 0.6
		iso-C_3H_7I	
Carl and Crowley[11]	LFP-RF	20 (Ar)[b]	12.2 ± 0.6
Cotter et al.[22]	FFD-RF	1.5 and 5.0 (He)[b]	16 ± 2
this work	FP-RF	188 (He)[b]	12.8 ± 0.7

[a]FFD-RF, fast flow discharge resonance fluorescence; LFP-RF, laser flash photolysis resonance fluorescence. [b]Buffer gas

k_1 at ambient temperature to be more than a factor of 2.3 lower than the value reported from a room-temperature kinetic study by Cotter et al. (2003).[22] These investigators used a fast flow discharge resonance fluorescence (FFD-RF) system to obtain $k_1(298\ K) = (7.7 \pm 1.0) \times 10^{-13}$ cm^3 molecule^{-1} s^{-1}.[22] Further, we found k_2 and k_3 at ambient temperature to be factors of 2.1 and 1.2 lower, respectively, than the values reported by Cotter et al.[22] based on room-temperature studies of reactions 2 and 3. The only other room-temperature kinetic studies of reactions 2 and 3 were carried out by Carl and Crowley (2001)[11] using a laser flash photolysis resonance fluorescence (LFP-RF) system. The ambient-temperature rate coefficient k_2 obtained in this work is a factor of 1.2 lower than that reported by Carl and Crowley, namely, $k_2(298\ K) = (14.7 \pm 0.8) \times 10^{-13}$ cm^3 molecule^{-1} s^{-1}.[11] The ambient-temperature rate coefficient k_3 obtained in this work agrees very well with $k_3(298\ K)$ obtained by Carl and Crowley.[11]

Whereas our kinetic results agree well with the data obtained by Carl and Crowley,[11] the kinetic results obtained by Cotter et al.[22] appear to be higher (see Figure 6). The overall accuracy of the obtained rate coefficients is determined by the accuracy of the alkyl iodide concentration measurements. Carl and Crowley and Cotter et al. used different techniques to calculate the alkyl iodide concentration. Specifically, Carl and Crowley[11] used a UV absorption technique, whereas Cotter et al.[22] calculated the alkyl iodide concentration by calculating a mixing ratio based on relative and total flow rates through mass flow controllers and the total pressure and then purified the mixtures by repeated freeze−pump−thaw cycles. In our work, the alkyl iodide concentration was obtained by calculating the mixing ratio based on vapor pressure data as a function of temperature, total flow rates through calibrated mass flow controllers, and the total pressure. However, at this point, we cannot conclude why the results obtained by Cotter et al.[22] are higher than those obtained by Carl and Crowley[11] and by us. Further studies will be required to resolve this issue.

No temperature-dependent kinetic data are available in the literature for comparison with the rate coefficients reported in this work. The obtained rate coefficients for reactions 1−3 increase slightly with temperature over the ranges measured. From the Arrhenius plot shown in Figure 6, the activation energies for the reactions OH + C_2H_5I, OH + n-C_3H_7I, and OH + iso-C_3H_7I were calculated to be 6.9 ± 1.5, 6.5 ± 1.5, and 4.4 ± 1.3 kJ mol^{-1}, respectively. The uncertainties are 2σ.

The room-temperature rate coefficients for reactions 1−3 obtained in this work are listed in Table 2. Also, we recently remeasured the temperature dependence of the OH + CH_3I reaction and measured for the first time the temperature dependence of the OH + CH_2I_2 reaction, obtaining $k_{OH+CH_3I}(298\ K) = 6.39 \times 10^{-14}$ cm^3 molecule^{-1} s^{-1} and $k_{OH+CH_2I_2}(298\ K) = 4.43 \times 10^{-12}$ cm^3 molecule^{-1} s^{-1}.[24,23] We found that all of the reactions of OH radical with the selected RIs exhibit a positive temperature dependence.

One potential source of a systematic error in the measured absolute rate coefficients is uncertainty in the vapor pressures used to calculate RI concentrations. Flow meter calibrations were checked frequently over the course of the study and are believed to be accurate to within a few percent. Further, to calculate RI concentrations, we used the Antoine equations taken from Stull.[31] The saturator that contained the C_2H_5I, n-C_3H_7I, and iso-C_3H_7I samples was maintained at −1.0 ± 0.5, 0.00 ± 0.5, and −6.0 ± 0.5 °C, respectively. The He was allowed to bubble through the liquid reactant for hours and days with no observable change in OH radical reactivity. As a result, we concluded that no impurities were present in the iodoalkanes with higher volatility. The temperature within the saturator was monitored using a type-J thermocouple (Omega). The thermocouple was calibrated externally with an ice/deionized water mixture and at several temperatures using a thermostatically controlled cooling bath (Fisher Scientific) (T < 25 °C) and a thermocouple calibration tube furnace (T < 25 °C). The uncertainty in the saturator temperature was calculated to be ±0.5 °C. As a result, we estimate the uncertainty in the RI concentrations to be ±3%

Another potential source of error in the measured rate coefficient is the potential loss of RI due to VUV photolysis to produce R radicals and I atoms

$$RI + h\nu\ (\lambda > 120\ nm) \rightarrow R + I \qquad (4')$$

$$R + OH \rightarrow \text{products} \qquad (5')$$

$$I + OH \rightarrow \text{products} \qquad (6)$$

As in the work of Nakano et al. (2006)[39] and our previous work,[23,24] the concentrations of R radicals and I atoms following VUV flash photolysis of the RI/H_2O/He mixtures were estimated from the photoabsorption cross sections in the wavelength range of interest

Table 3. List of Reactions Used to Simulate the OH Radical Temporal Decays Following RI Photolysis

	reaction	k(298 K) (cm^3 molecule^{-1} s^{-1})	ref
	$C_2H_5I + h\nu \rightarrow C_2H_5 + I$		
(7)	$C_2H_5 + H \rightarrow C_2H_6$ (undefined)	1.7×10^{-10}	42
(8)	$C_2H_5 + I \rightarrow C_2H_5I$ (undefined)	1.2×10^{-11}	43
(9)	$C_2H_5 + OH \rightarrow$ products (undefined)	1.2×10^{-10}	44
(10)	$C_2H_6 + OH \rightarrow$ products (undefined)	1.2×10^{-12}	45
(11)	$C_2H_5 + C_2H_5 \rightarrow$ products (undefined)	2.3×10^{-11}	46
(12)	$C_2H_5 + O_2 \rightarrow$ products (undefined)	1.0×10^{-12}	47
	n-/iso-$C_3H_7I + h\nu \rightarrow C_3H_7 + I$		
(13)	$C_3H_7 + H \rightarrow C_3H_8$ (undefined)	2.5×10^{-10}	48
(14)	$C_3H_7 + I \rightarrow C_3H_7I$ (undefined)	1.2×10^{-11}	43[b]
(15)	$C_3H_7 + OH \rightarrow$ products (undefined)	4.0×10^{-11}	49
(16)	$C_3H_8 + OH \rightarrow$ products (undefined)	1.1×10^{-12}	50
(17)	$C_3H_7 + C_3H_7 \rightarrow$ products (undefined)	1.7×10^{-11}	51
(18)	$C_3H_7 + O_2 \rightarrow$ products (undefined)	8.0×10^{-12}	52
	Additional Reactions		
(6)	$I + OH \rightarrow$ products (undefined)	8.9×10^{-25}	53[c]
(20)	$OH + OH \rightarrow H_2O + O$ (undefined)	1.5×10^{-12}	54
(21)	$H + O_2 \rightarrow OH + O$ (undefined)	7.6×10^{-22}	55
(22)	$O + OH \rightarrow O_2 + H$ (undefined)	1.5×10^{-12}	54
(23)	$OH + H \rightarrow H_2O$ (undefined)	1.6×10^{-31}	56
(24)	$H + O_2 \rightarrow HO_2$ (undefined)	7.5×10^{-11}	57
(25)	$H + HO_2 \rightarrow 2OH$ (undefined)	7.2×10^{-11}	54
(26)	$O + HO_2 \rightarrow OH + O_2$ (undefined)	5.8×10^{-11}	54

[b]It was assumed that the room-temperature rate coefficient for $C_3H_7 + I$ is the same as that for $C_2H_5 + I$ (see text). [c]It was assumed that the room-temperature rate coefficient for $I + OH$ is the same as that for $Br + OH$ (see text).

$$[R]_0 \approx [I]_0 \approx [OH]_0 \frac{\sigma_{RI}[RI]}{\sigma_{H_2O}[H_2O]} \quad \text{(VIII)}$$

In eq VIII, $\sigma_{C_2H_5I}$, $\sigma_{n\text{-}C_3H_7I}$, $\sigma_{iso\text{-}C_3H_7I}$, and σ_{H_2O} were taken to be 1.57×10^{-16},[40] 7.00×10^{-18},[40] 7.59×10^{-17},[40] and 5×10^{-18} cm^2,[35] respectively, as determined at the Xe resonance line at 147 nm.[40] The initial C_2H_5 and I concentrations ($[C_2H_5]_0$ and $[I]_0$, respectively) were calculated to be 1.7×10^{11} molecules cm^{-3} following the VUV flash photolysis of the C_2H_5I/H_2O/He mixtures. The initial C_3H_7 and I concentrations ($[C_3H_7]_0$ and $[I]_0$, respectively) were calculated to be 1.9×10^9 molecules cm^{-3} following the VUV flash photolysis of the n-C_3H_7I/H_2O/He mixtures. The initial C_3H_7 and I concentrations ($[C_3H_7]_0$ and $[I]_0$, respectively) were calculated to be 2.0×10^{10} molecules cm^{-3} following the VUV flash photolysis of the iso-C_3H_7I/H_2O/He mixtures. To estimate the influence of reactions 5 and 6 on the initial OH concentration, the OH radical consumption was simulated using the COPASI 4.6 (build 32) simulator for biochemical networks.[41] All additional reactions that were used to simulate the OH radical temporal decays following RI photolysis are listed in Table 3. Modeled OH radical consumption resulting from possible VUV photolysis of C_2H_5I, n-C_3H_7I, and iso-C_3H_7I are shown in Figure 7. It was assumed that VUV photolysis of both n-C_3H_7I, and iso-C_3H_7I yields C_3H_7 radicals and I atoms with no difference in mechanism. In Figure 7, decay path ($C_2H_5I + h\nu$) includes reactions 6, 7−12, and 20−26, and decay path ($C_2H_5I + h\nu + OH$) includes reaction 1 in addition to the previously listed reactions. Further, OH radical consumption path ($C_3H_7I + h\nu$) includes reactions 6, 13−18, and 20−26, and OH radical consumption pathways (iso-$C_3H_7I + h\nu + OH$) and (n-$C_3H_7I + h\nu + OH$) include reactions 3 and 2, respectively, in addition to the previously listed reactions. Initial H-atom, C_2H_5, and C_3H_7 radical concentrations were calculated using eq VIII. No kinetic data are available in the literature for the reaction $I + C_3H_7$. It was thus assumed that the room-temperature rate coefficient for this reaction is the same as that for the corresponding reaction of C_2H_5 radical with an I atom ($k_{C_2H_5+I} = 1.16 \times 10^{-11}$ cm^3 molecule^{-1} s^{-1}).[43] Further, no room-temperature rate coefficient values have been reported in the literature for the reaction of OH radicals with I atoms, so it was assumed that the room-temperature rate coefficient for this reaction is the same as that for OH + Br ($k_{OH+Br} = 8.94 \times 10^{-25}$ cm^3 molecule^{-1} s^{-1}).[40] Based on model calculations, OH radicals were observed to be consumed primarily by reactions 1−3, and OH radical loss through the reactions listed in Table 3 was calculated to be about 16%, 6%, and 11% for C_2H_5I, n-C_3H_7I, and iso-C_3H_7I, respectively.

The reactions of OH radicals with short-chain alkyl iodides, namely, CH_3I, CH_2I_2, C_2H_5I, n-C_3H_7I, and iso-C_3H_7I have been suggested to proceed through H-atom abstraction.[22] Marshall et al. (1997) used the Gaussian-2 level of theory to study the $^{\bullet}OH + CH_3I$ reaction and predicted H-atom abstraction channel faster than HOI formation (I-atom abstraction).[58] More recently, Louis et al. (2011) used a high-level all-electron ab initio DK-CCSD(T)/ANO-RCC approach to compare the

dx.doi.org/10.1021/jp300575f | J. Phys. Chem. A 2012, 116, 9497−9506

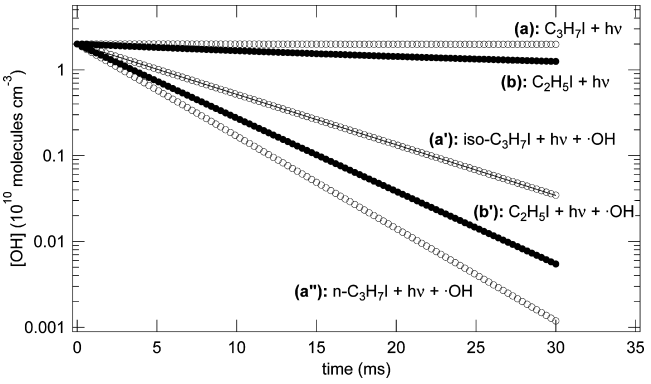

Figure 7. Model results for potential loss of C_2H_5I, *n*-C_3H_7I, and iso-C_3H_7I due to VUV photolysis to produce C_2H_5 and C_3H_7 radicals and I atoms. Initial I atom and C_2H_5 and C_3H_7 radical concentrations were calculated using equation eq VIII. (a) OH radical consumption calculated using reactions 6, 7−12, and 20−26 listed in Table 3 that results in a decay rate of 31 s^{-1}. (a′) OH radical consumption calculated using reaction 3 in addition to reactions 6, 13−18, and 20−26 listed in Table 3 that results in a decay rate of 135 s^{-1}. The decay rate ratio yields an 11% difference in the OH radical consumption due to VUV photolysis of iso-C_3H_7I. (a″) OH radical consumption calculated using reaction 2 in addition to reactions 6, 13−18, and 20−26 listed in Table 3 that results in a decay rate of 247 s^{-1}. The decay rate ratio yields a 6% difference in the OH radical consumption due to VUV photolysis of *n*-C_3H_7I. (b) OH radical consumption calculated using reactions 6, 7−12, and 20−26 listed in Table 3 that results in a decay rate of 31 s^{-1}. (b′) OH radical consumption calculated using reaction 1 in addition to reactions 6, 7−12, and 20−26 listed in Table 3 that results in a decay rate of 199 s^{-1}. The decay rate ratio yields a 16% difference in the OH radical consumption due to VUV photolysis of C_2H_5I.

H-atom and I-atom abstraction channels for the •OH + CH_3I and •OH + CH_2I_2 reactions. These investigators predicted the I-atom abstraction (in contrast to the H-atom abstraction) transition state to be below the reaction products and calculated the H-atom abstraction channel to be strongly exothermic (between −80 and −90 kJ mol^{-1}) and the I-atom abstraction channel to be endothermic (between +20 and +40 kJ mol^{-1}). This is best explained by the difference in the C−H and C−I bond strengths, which are 431 and 239 kJ mol^{-1}, respectively.[59] Whether an iodine atom is released from the OH attack depends on the location of the H-atom abstraction with respect to the location of the C−I bond. Cotter et al. predicted that, if H-atom abstraction occurs at a hydrogen bonded to C−I, iodine atom release should be expected.[5] If H-atom abstraction occurs at a site other than C−I, then iodoalkyl radical production should be expected.[22] It has been suggested that the presence of the I atom results in a weakening of the neighboring C−H bonds, as seen for the reactions of OH radicals with CH_3I ($k = 6.4 \times 10^{-14}$ cm^3s^{-1} at 298 K) and CH_4 ($k = 6.3 \times 10^{-15}$ cm^3s^{-1} at 298 K).[60] Further, it was observed that the substitution of a methyl group at one of the carbon atoms of the double bond on ethene increases substantially the rate of the reaction; that is, the rate is three times larger in propene than in ethene and twice as large in methyl propene as in propene.[61] Also, the position at which the methyl group is substituted seems to be less important. Therefore, a dependence seems to exist between the rate of the reaction and the electronic dipolar effects due to the substituents.[61] The dipole moments and ionization potentials for selected short-chain alkyl iodides are listed in Table 4. It can be seen that, for CH_3I and CH_2I_2, the reaction rates exhibit a negative dependence on the dipole moment and ionization potential. This seems to be expected in an H-atom abstraction mechanism if one considers that the presence of the I atoms results in a weakening of the C−H bond in the CH_xI_y molecule. It is not surprising to observe that the rate coefficient for the OH + C_2H_5I reaction ($k = 3.62 \times 10^{-13}$ cm^3s^{-1} at 298 K) is larger than the rate coefficient for the OH + CH_3I reaction ($k = 6.4 \times 10^{-14}$ cm^3s^{-1} at 298 K). However, it is somewhat unexpected to observe that the rate coefficient for the OH + C_2H_5I reaction is lower than the rate coefficients for the OH + CH_2I_2 reaction ($k = 4.42 \times 10^{-12}$ cm^3s^{-1} at 298 K). As discussed by Alvarez-Idaboy et al., substitution of a methyl group at one of the carbon atoms does increase the rate of the reaction in alkenes but it is the I atom that weakens the C−H bond and leads to a substantial increase in the rate coefficient. Addition of the CH_3 group does not weaken the C−H bond significantly to have a considerable effect on the reaction rate.

Table 4. Dipole Moments and Ionization Potential Values for CH_3I, CH_2I_2, C_2H_5I, *n*-C_3H_7I, and iso-C_3H_7I

RI	dipole moment (D)	ionization potential (eV)	k_{OH}(298 K) (10^{-12} cm^3 s^{-1})
CH_3I	1.711	9.54	0.064 ± 0.006
CH_2I_2	1.538	9.46	4.43 ± 0.30
C_2H_5I	1.905	9.35	0.362 ± 0.034
n-C_3H_7I	1.938	9.26	1.24 ± 0.6
iso-C_3H_7I	2.045	9.19	1.35 ± 0.7

In Table 4, the dipole moment was calculated based on geometry optimization using an ab initio method: STO-3G, restricted Hartree−Fock spin pairing, Polak−Ribière (conjugate-gradient) optimization.

The reactions of OH radicals with *n*-C_3H_7I and iso-C_3H_7I were studied at 298 K by Carl and Crowley.[11] They observed the rate for the OH + *n*-C_3H_7I reaction to be 20% larger than that for the OH + iso-C_3H_7I reaction. In contrast to the work of Carl and Crowley,[11] we measured the room-temperature rate coefficient for the OH + *n*-C_3H_7I reaction ($k = 1.24 \times 10^{-12}$ cm^3s^{-1} at 298 K) to be more that 10% lower than the room-temperature rate coefficient for the OH + iso-C_3H_7I reaction ($k = 1.35 \times 10^{-12}$ cm^3s^{-1} at 298 K). This is probable if one considers that the overall rate of H-atom abstraction is a factor of 4 higher for the CH_2 group in propane than for CH_3 groups,[62] implying a 298 K rate coefficient of 3.7×10^{-14} cm^3 s^{-1} per primary H atom and 4.4×10^{-13} cm^3s^{-1} per secondary H atom. Similarly, replacing the secondary H atom with I results in a weaker neighboring C−H bond in iso-C_3H_7I compared to the two weaker neighboring C−H bonds in *n*-C_3H_7I. A dependence seems to exist between the rate of the reaction and the geometric factors. Another explanation is that the reactions of OH radicals with alkyl iodides partially proceed through a complex mechanism in which OH radical attack at the C−I bond proceeds in a manner similar to the reaction of $O(^3P)$ with alkyl iodides.[13,63] There is theoretical evidence supporting such an OH-complex mechanism for OH + haloethanes reactions.[64] Consequently, formation of an OH complex leading to I-atom abstraction cannot be excluded.

As a result, although strong arguments exist that predict the reaction of OH radicals with alkyl iodides to proceed through H-atom abstraction to give H_2O and an iodine-containing alkyl radical as products, the formation of an OH complex cannot be excluded. Studying specific reaction channels and/or direct

dx.doi.org/10.1021/jp300575f | J. Phys. Chem. A 2012, 116, 9497−9506

detection of HOI and IO radical products would clarify this issue. Further, IO and HOI are known to participate in aerosol formation. Because many organic-iodide destruction pathways to form IO and condensable HOI remain uncertain and unknown, it behooves the atmospheric community to study these reaction mechanisms to better understand aerosol formation. Clearly, further research into this subject is warranted.

CONCLUSIONS

The results reported in this work demonstrate that $k_1(T)$, $k_2(T)$, and $k_3(T)$, the rate coefficients for the reaction of OH radicals with C_2H_5I, n-C_3H_7I, and iso-C_3H_7I, respectively, are $k_1(297-372\ K) = (5.55 \pm 3.20) \times 10^{-12} \exp[-(830 \pm 90)\ K/T]$, $k_2(300-370\ K) = (1.65 \pm 0.90) \times 10^{-11} \exp[-(780 \pm 90)\ K/T]$, and $k_3(299-369\ K) = (7.58 \pm 3.70) \times 10^{-12} \exp[-(530 \pm 80)\ K/T]$ cm^3 molecule^{-1} s^{-1} over the measured temperature ranges. For the three title reactions this work represents the first study of the temperature dependence of the rate. Reactions 1−3 exhibit an increase in the measured rate coefficient with increasing temperature. The positive temperature dependence of k_1, k_2, and k_3 indicates that the three reactions have an activation barrier.

Atmospheric Implications. Atmospheric sinks of iodoalkanes include photolysis and reactions with OH radicals and O(^{3}P) and Cl atoms. A comparison of the relative magnitudes of the different loss rates toward phtolysis and attacks by OH, O(^{3}P), and Cl is shown in Table 5.

Table 5. Atmospheric Lifetimes (in Hours) at T = 298 K of C_2H_5I, n-C_3H_7I, and iso-C_3H_7I in the Marine Boundary Layer, with Respect to Photolysis and Reactions with O(^{3}P), OH, and Cl[a,b]

RI	photolysis[c]	O(^{3}P)[d]	OH[e]	Cl[f]
C_2H_5I	132	39	772	3470
n-C_3H_7I	99	37	224	842
iso-C_3H_7I	50	28	206	1208

[a]Lifetimes toward photolysis and attacks by O, OH, and Cl radicals calculated as J^{-1}, $1/(k_{O+RI}[O])$, $1/(k_{OH+RI}[OH])$, and $1/(k_{Cl+RI}[Cl])$, respectively. [b]Atmospheric concentrations used to calculate RI lifetimes taken to be $[O(^3P)] = 2 \times 10^5$ molecules cm^{-3}, $[OH] = 1 \times 10^6$ molecules cm^{-3}, and $[Cl] = 5 \times 10^3$ molecules cm^{-3}. [c]Daylight average photolysis rates taken from Cotter et al.[5] [d]$k_{O(^3P)+C_2H_5I} = 3.52 \times 10^{-11}$, $k_{O(^3P)+n\text{-}C_3H_7I} = 3.77 \times 10^{-11}$, and $k_{O(^3P)+iso\text{-}C_3H_7I} = 5.18 \times 10^{-11}$ cm^3 molecule^{-1} s^{-1}.[63] [e]$k_{OH+C_2H_5I} = 3.62 \times 10^{-13}$, $k_{OH+n\text{-}C_3H_7I} = 12.4 \times 10^{-13}$, and $k_{OH+iso\text{-}C_3H_7I} = 13.5 \times 10^{-13}$ cm^3 molecule^{-1} s^{-1} measured at T = 298, 300 and 299K, respectively. This work. [f]$k_{Cl+C_2H_5I} = 16 \times 10^{-12}$, $k_{Cl+n\text{-}C_3H_7I} = 66.5 \times 10^{-12}$, and $k_{Cl+iso\text{-}C_3H_7I} = 46.8 \times 10^{-12}$ cm^3 molecule^{-1} s^{-1}.[5]

It was assumed that the MBL daylight average values of concentrations were $[OH] = 1 \times 10^6$ molecules cm^{-3},[65] $[Cl] = 5 \times 10^3$ atoms cm^{-3},[66] and $[O(^3P)] = 2 \times 10^5$ atoms cm^{-3}. As shown in Table 5, the MBL losses of C_2H_5I, n-C_3H_7I, and iso-C_3H_7I are predominantly governed by reactions of O(^{3}P) atoms and photolysis, but OH radical reactions gain importance with substituted propanes. The reactions of OH radicals with C_2H_5I, n-C_3H_7I, and iso-C_3H_7I most likely proceed through H-atom abstraction, producing iodoalkyl radical that ultimately will lead to release of iodine and the production of HO_x.[5]

Nuclear Field Implications. If a major nuclear power plant accident were to occur, the OH radical concentration in the reactor containment would be about 1000 times higher than the natural atmospheric OH radical concentration.[21] Therefore, under the conditions resulting from such a nuclear power plant accident, the lifetimes of C_2H_5I, n-C_3H_7I, and iso-C_3H_7I toward destruction by OH radicals would be approximately 46, 13, and 12 min, respectively. Including previous results obtained with CH_3I and CH_2I_2, interactions with O and OH radicals can be expected to be the dominant effect in RI destruction into iodine oxides.[24,23] Nevertheless, in this work, we used VUV radiation as a photolytic light source for creating OH radicals. For nuclear applications, effects of β- and γ-radiation produced by fission products on both the direct destruction of RIs and the production of oxidant radicals other than O$^\bullet$ and OH$^\bullet$ remain to be investigated. This will be done in the near future by considering the few experiments available on RI destruction by radiolysis in both neutral and most air atmospheres.[67]

AUTHOR INFORMATION

Corresponding Author

*E-mail: rafal.strekowski@univ-amu.fr. Phone: (+33) (0)4 13 55 10 40. Fax: (+33) (0)4 13 55 10 60.

Notes

The authors declare no competing financial interest.

ACKNOWLEDGMENTS

Financial support from the Institut de Radioprotection et de Sûreté Nucléaire (IRSN) is gratefully acknowledged. C.Z. thanks the German Science Foundation for support within research unit 763 (HaloProc) and the EU for support within the infrastructure EUROCHAMP. S.Z. and R.S.S. also thank the EU for support within the infrastructure EUROCHAMP.

REFERENCES

(1) Chameides, W.; Davis, D. *J. Geophys. Res.* **1980**, *85*, 7383−7398.
(2) Wayne, R. P. *Chemistry of Atmospheres*; Oxford University Press: Oxford, U.K., 2000.
(3) Vogt, R.; Sander, R.; Von Glasow, R.; Crutzen, P. J. *J. Atmos. Chem.* **1999**, *32*, 375−395.
(4) Alicke, B.; Hebestreit, K.; Stutz, J.; Platt, U. *Nature* **1999**, *397*, 572−573.
(5) Cotter, E.; Booth, N.; Canosa-Mas, C.; Gray, D.; Shallcross, D.; Wayne, R. *Phys. Chem. Chem. Phys.* **2001**, *3*, 402−408.
(6) Davis, D.; Crawford, J.; Liu, S.; McKee, S.; Bandy, A.; Thornton, D.; Rowland, F.; Blake, D. *J. Geophys. Res.* **1996**, *101*, 2135−2147.
(7) Jones, C. E.; Hornsby, K. E.; Dunk, R. M.; Leigh, R. J.; Carpenter, L. J. *Atmos. Chem. Phys.* **2009**, *9*, 8757−8769.
(8) Martino, M.; Mills, G. P.; Woeltjen, J.; Liss, P. S. *Geophys. Res. Lett.* **2009**, *36*, L01609.
(9) Solomon, S.; Garcia, R. R.; Ravishankara, A. R. *J. Geophys. Res.* **1994**, *99*, 20491.
(10) Schall, C.; Heumann, K. G. *Fresenius' J. Anal. Chem.* **1993**, *346*, 717−722.
(11) Carl, S. A.; Crowley, J. N. *Atmos. Chem. Phys.* **2001**, *1*, 1−7.
(12) Cotter, E. S. N.; Booth, N. J.; Canosa-Mas, C.; Wayne, R. *Atmos. Environ.* **2001**, *35*, 2169−2178.
(13) Gilles, M. K.; Turnipseed, A. A.; Talukdar, R. K.; Rudich, Y.; Villalta, P. W.; Huey, L. G.; Burkholder, J. B.; Ravishankara, A. R. *J. Phys. Chem.* **1996**, *100*, 14005−14015.
(14) Orlando, J.; Piety, C.; Nicovich, J.; McKee, M.; Wine, P. *J. Phys. Chem. A* **2005**, *109*, 6659−6675.
(15) Carr, R. W., Jr.; Topor, M. G. *J. Photochem.* **1981**, *16*, 51−65.
(16) Hayes, D. M.; Strong, R. L. *J. Phys. Chem.* **1986**, *90*, 6305−6309.

(17) Deshmukh, S.; Brum, J. L.; Koplitz, B. *Chem. Phys. Lett.* **1991**, *76*, 198−202.
(18) Ball, J. M.; Glowa, G. A.; Boulianne, D.; Mitchell, J. R. *Behaviour of Iodine Project: Final Report on Organic Iodide Studies*; Nuclear Energy Agency, Atomic Energy of Canada Limited: Chalk River, Ontario, Canada, 2011
(19) Bosland, L.; Funke, F.; Girault, N.; Langrock, G. *Nucl. Eng. Des.* **2008**, *238*, 3542.
(20) Bosland, L.; Funke, F.; Langrock, G.; Girault, N. *Nucl. Eng. Des.* **2011**, *241*, 4026.
(21) Sims, H. E. *Modifications to the IODAIR Model for Gas Phase Iodine Radiation Chemistry*; NNL/BE00728/06/10/172 NRS/CHEM/BEGL/P(09)056, Issue 1, National Nuclear Laboratory Technical Report, U.K., 2009.
(22) Cotter, E.; Canosa-Mas, C.; Manners, C.; Wayne, R.; Shallcross, D. *Atmos. Environ.* **2003**, *37*, 1125−1133.
(23) Zhang, S.; Strekowski, R.; Bosland, L.; Monod, A.; Zetzsch, C. *Phys. Chem. Chem. Phys.* **2011**, *13*, 11671−11677.
(24) Zhang, S.; Strekowski, R.; Bosland, L.; Monod, A.; Zetzsch, C. *Int. J. Chem. Kinet.* **2011**, *43*, 547−556.
(25) Rinke, M.; Zetzsch, C. *Ber. Bunsen-Ges. Phys. Chem.* **1984**, *88*, 55−62.
(26) Stuhl, F.; Niki, H. *J. Chem. Phys.* **1972**, *57*, 3677−3679.
(27) Witte, F.; Urbanik, E.; Zetzsch, C. *J. Phys. Chem.* **1986**, *90*, 3250−3259.
(28) Wahner, A.; Zetzsch, C. *J. Phys. Chem.* **1983**, *87*, 4945−4951.
(29) Davis, D.; Braun, W. *Appl. Opt.* **1968**, *7*, 2071−2074.
(30) Aldrich, E. W.; Bridgeman, O. C. *J. Heat Transfer* **1964**, *86*, 279−286.
(31) Stull, D. R. *Ind. Eng. Chem.* **1947**, *39*, 517−540.
(32) Dusanter, S.; Vimal, D.; Stevens, P. S. *Atmos. Chem. Phys. Discuss.* **2007**, *7*, 12877−12926.
(33) Faloona, I. C.; Tan, D.; Lesher, R. L.; Hazen, N. L.; Frame, J. B.; Simpas, C.; Harder, H.; Martinez, M.; Di Carlo, P.; Ren, X.; Brune, W. H. *J. Atmos. Chem.* **2004**, *47*, 139−167.
(34) Sander, S. P.; Friedl, R. R.; Golden, D. M.; Kurylo, M. J.; Moortgat, G. K.; Keller-Rudek, H.; Wine, P. H.; Ravishankara, A. R.; Kolb, C. E.; Molina, M. J.; Finlayson-Pitts, B. J.; Huie, R. E.; Orkin, V. L. *Chemical Kinetics and Photochemical Data for Use in Atmospheric Studies Evaluation 15*; California Institute of Technology: Pasadena, CA, 2006.
(35) Okabe, H. *Photochemistry of Small Molecules*; Wiley: New York, 1978.
(36) Heard, D. E.; Pilling, M. J. *Chem. Rev.* **2003**, *103*, 5163−5198.
(37) Holland, F.; Hofzumahaus, A.; Schäfer, J.; Kraus, A.; Pätz, H. W. *J. Geophys. Res.* **2003**, *108*, 8246.
(38) Dubey, M. K.; Mohrschladt, R.; Donahue, N. M.; Anderson, J. G. *J. Phys. Chem. A* **1997**, *101*, 1494−1500.
(39) Nakano, Y.; Ukeguchi, H.; Ishiwata, T. *Chem. Phys. Lett.* **2006**, *430*, 235−239.
(40) Rebbert, R. E.; Lias, S. G.; Ausloos, P. *Int. J. Chem. Kinet.* **1973**, *5*, 893−908.
(41) *COPASI Simulator for Biochemical Networks*, Copyright 2005 by Pedro Mendes; Virginia Tech Intellectual Properties, Inc. and EML Research, gGmbH, November 2011; http://www.copasi.org.
(42) Sillesen, A.; Ratajczak, E.; Pagsberg, P. *Chem. Phys. Lett.* **1993**, *201*, 171−177.
(43) Hunter, T.; Kristjansson, K. *J. Chem. Soc., Faraday Trans. 2* **1982**, *78*, 2067−2076.
(44) Fagerstrom, K.; Lund, A.; Mahmoud, G.; Jodkowski, J.; Ratajczak, E. *Chem. Phys. Lett.* **1993**, *208*, 321−327.
(45) Anderson, R. S.; Huang, L.; Iannone, R.; Thompson, A.; Rudolph, J. *J. Phys. Chem. A* **2004**, *108*, 11537−11544.
(46) Adachi, H.; Basco, N.; James, D. G. L. *Int. J. Chem. Kinet.* **1979**, 11.
(47) Slagle, I. R.; Feng, Q.; Gutman, D. *J. Phys. Chem.* **1984**, 88.
(48) Munk, J.; Pagsberg, P.; Ratajczak, E.; Sillesen, A. *Chem. Phys. Lett.* **1986**, 132.
(49) Tsang, W. *J. Phys. Chem. Ref. Data* **1988**, *17*, 887−951.
(50) Kozlov, S. N.; L., O. V.; Huie, R. E.; Kurylo, M. J. *J. Phys. Chem. A* **2003**, *107*, 1333−1338.
(51) Adachi, H.; Basco, N. *Int. J. Chem. Kinet.* **1981**, *13*, 367−384.
(52) Atkinson, R.; Baulch, D. L.; Cox, R. A.; Hampson, J., R. F.; Kerr, J. A.; Rossi, M. J.; Troe, J. *J. Phys. Chem. Ref. Data* **1997**, *26*, 521−1011.
(53) Baulch, D. L.; Duxbury, J.; Grant, S. J.; Montague, D. C. *J. Phys. Chem. Ref. Data.* Vol. 10, Supplement No. 1: 1981, 721 pages, ISBN 0-88318-281-5.
(54) Atkinson, R.; Baulch, D.; Cox, R.; Crowley, J.; Hampson, R.; Hynes, R.; Jenkin, M.; Rossi, M.; Troe, J. *Atmos. Chem. Phys.* **2004**, *4*, 1461−1738.
(55) Baulch, D.; Cobos, C.; Cox, R.; Frank, P.; Hayman, G.; Just, T.; Kerr, J.; Murrells, T.; Pilling, M.; Troe, J.; Walker, R.; Warnatz, J. *J. Phys. Chem. Ref. Data* **1994**, *23*, 847−1033.
(56) Zellner, R.; Erler, K.; Field, D. *Symp. Int. Combust. Proc.* **1977**, 16.
(57) DeMore, W. B.; Sander, S. P.; Golden, D. M.; Hampson, R. F.; Kurylo, M. J.; Howard, C. J.; Ravishankara, A. R.; Kolb, C. E.; Molina, M. J. *Chemical Kinetics and Photochemical Data for Use in Stratospheric Modeling*; Evaluation No. 12, JPL Publication 97-4; Jet Propulsion Laboratory: Pasadena, CA, 1997.
(58) Marshall, P.; Misra, A.; Berry, R. J. *Chem. Phys. Lett.* **1997**, *265*, 48−54.
(59) Louis, F.; Černušák, I.; Canneaux, S.; MeČiarovaá, K. *Computational and Theoretical Chemistry* **2011**, *965*, 275−284.
(60) Sander, S. P.; Abbatt, J.; Barker, J. R.; Burkholder, J. B.; Friedl, R. R.; Golden, D. M.; Huie, R. E.; Kolb, C. E.; Kurylo, M. J.; Moortgat, G. K.; Orkin, V. L.; Wine, P. H. *Chemical Kinetics and Photochemical Data for Use in Atmospheric Studies*; Evaluation No. 17, JPL Publication 10-6; Jet Propulsion Laboratory: Pasadena, CA, 2011.
(61) Alvarez-Idaboy, J. R.; Mora-Diez, N.; Vivier-Bunge, A. *J. Am. Chem. Soc.* **2000**, *122*, 3715−3720.
(62) Talukdar, R. K.; Mellouki, A.; Gierczak, T.; Barone, S.; Chiang, S.-Y.; Ravishankara, A. R. *Int. J. Chem. Kinet.* **1994**, *26*, 973.
(63) Teruel, M. A.; Dillon, T. J.; Horowitz, A.; Crowley, J. N. *Phys. Chem. Chem. Phys.* **2004**, *6*, 2172−2178.
(64) Sekusak, S.; Sabljic, A. *Chem. Phys. Lett.* **1997**, *272*, 353−360.
(65) Prinn, R. G.; Weis, R. F.; Miller, B. R.; Huang, J.; Alyea, F. N.; Cunnold, D. M.; Fraser, P. J.; Hartley, D. E.; Simmonds, P. G. *Science* **1995**, *269*, 169−172.
(66) Singh, H. B.; Kasting, J. F. *J. Atmos. Chem.* **1988**, *7*, 261−286.
(67) Donovan, J. M.; Hanrahan, R. J. *Int. J. Radiat. Phys. Chem.* **1971**, *3*, 491−501.